Identification of Vehicular Axle Weights with a BWIM System Considering Transverse Distribution of Wheel Loads

Hua Zhao[1], Ph.D.; Nasim Uddin, Ph.D., P.E., F.ASCE[2]; Eugene J. O'BRIEN[3], Ph.D.; Xudong Shao[4], Ph.D.

Abstract: A modified 2-D Moses algorithm for acquiring the field-calibrated influence line (IL) of an existing bridge is presented, based on strain data acquired continuously at a high scanning rate with calibration vehicles of known axle weights and axle spacings crossing an instrumented bridge. Considering the transverse distribution of the wheel loads on each girder due to two-dimensional (2-D) behavior of slab-girder bridge, the ILs of each of the girders can be calculated, which does not require the girders to possess the identical material and geometrical properties. By using the calculated ILs of each girder as references, a modified 2-D Moses algorithm was derived to identify axle weights of moving vehicles, taking into consideration the transverse distribution of the wheel loads on each girder. Mathematical equations to calculate ILs and axle weights were derived, and the proposed algorithms were implemented by a computer program written in MATLAB. The accuracy of the ILs calculation and axle weight identification was verified through a field test of a bridge on highway US-78 in Alabama. The identified axle weights showed agreement with the static measurements from weighing pads and with results from the bending-plate weigh-in-motion (BPWIM) system near the instrumented bridge.

CE Database subject headings: Bridge weigh-in-motion, influence line, axle weight, transverse distribution of wheel loads, inverse algorithm, bridge experiment

[1] Assistant Professor, Department of Bridge Engineering, Hunan University, Changsha, Hunan, 410082, China.; Research Associate, Department of Civil, Construction, and Environmental Engineering, University of Alabama at Birmingham, USA. (corresponding author) E-mail: zhmit@hotmail.com

[2] Professor, Department of Civil, Construction, and Environmental Engineering, University of Alabama at Birmingham, 1075 13th Street South, Birmingham, AL, 35294, USA. E-mail: nuddin@uab.edu

[3] Professor, School of Architecture, Landscape & Civil Engineering, University College Dublin, Belfield, Dublin 4, Ireland, Email: eugene.obrien@ucd.ie

[4] Professor, Department of Bridge Engineering, Hunan University, Changsha, Hunan, China. E-mail: shaoxd@hnu.edu.cn

Introduction

The safety of existing bridges can be accurately and reliably assessed if judgments are based on the actual resistance and the traffic (current and lifetime) expected over the structure. Decisions based on the acquisition of real live loads and accurate assessments of existing bridges will result in decreasing severe and expensive rehabilitation measures.

Recently developed bridge weigh-in-motion (BWIM) systems are portable devices capable of reliably delivering accurate measurements of vehicle type, size, and weight from moving vehicles. These systems are particularly suitable for short-term measurements, since they can be easily installed and can be relocated to other bridges. To obtain axle weights and gross vehicle weights (GVWs) of heavy trucks, BWIM systems use an instrumented bridge as a large sensor, and the transducers are mounted on the soffits of each girder along a line parallel to the longitudinal direction of the bridge (Moses, 1979; COST 323, 1999). A BWIM system increases the length of the load-sensitive element and thereby reduces the dynamic effects on accuracy relative to pavement WIM systems, where measurement of an axle lasts only a few milliseconds (ZAG, 2005).

In detecting vehicles, most of the current, conventional BWIM systems require pneumatic tubes or tape switches installed on the pavement of each lane of interest to provide vehicle silhouettes and velocities. A recently developed, innovative BWIM system replaces traditional systems with axle detector technology named like "nothing on the road (NOR)" or "free-of-axle detector (FAD)" (ZAG, 2005). This technology requires additional transducers mounted underneath the bridge slab to acquire dynamic signals of bridge with vehicles passing the instrumented bridge so as to characterize the vehicles. The BWIM system can be installed without interrupting traffic, and the system is invisible to truckers, thus preventing the drivers of heavy vehicles from deviating from their routes. In addition, as the BWIM system is portable and can be reapplied on other bridges, the cost is low in comparison with the pavement counterparts. As the BWIM system continuously records dynamic strain data of bridge response with vehicles passing the instrumented bridge, the system also supplies information about the dynamic impact factor, lateral distribution factor, and dynamic response of bridges, which can be further used for the assessment of the existing bridges (ZAG, 2005).

Since Moses (1979) first developed the concept of the BWIM system, many theoretical approaches to BWIM have been developed (Peters, 1984, 1986; Matui and El-Hakim, 1989; Quilligan et al, 2002; González and O'Brien, 1998; Leming and Stalford, 2003). For the application of BWIM system, many researchers made significant contributions (Snyder, 1992; Dempsey et al., 1995; O'Brien et al., 1999; Žnidarič and Baumgartner, 1998; Ojio et al., 2000, Jacob, 2010, González, 2010, Žnidarič et al, 2011, González et al, 2012). In order to predict axle loads with sufficient accuracy, especially for the close-spaced axle combinations of tandems, semitrailers, and trailers, Ojio et al. (2000) applied the BWIM concept to an orthotropic steel deck by calibrating the longitudinal stiffener in lieu of calibrating the whole bridge as a large sensor in the conventional BWIM algorithm. Xiao et al. (2006) also proposed a new method to obtain the axle weights of moving trucks by instrumenting the longitudinal ribs of an orthotropic box-girder bridge. By adding an additional regularization term in Moses' least-square formulation, Rowley et al. (2008) applied Tikhonov regularization method to the original least-square method to solve the ill-conditioned problem.

The BWIM algorithm takes the calculated or theoretical influence line (IL) as a reference. Obtaining an IL to represent realistic structural behavior under actual conditions is essential for successful application of the BWIM system. Many researchers attempted to calculate realistic IL coordinates based on measured bridge responses, or to adjust the theoretical ILs to make the modified ILs closer to the actual conditions to represent the bridge behavior in sufficient accuracy (ZAG, 2005; Žnidarič et al., 2002, 2011; McNulty and O'Brien, 2003; O'Brien et al, 2006). These approaches assume that the bridge behaves as a single beam, and the transverse load distribution characteristics are routinely ignored. The results, however, do not relate well to actual bridge behavior.

The present paper presents a field-calibrated algorithm to calculate ILs based on the measured strain data from a field test on a bridge on highway US-78 in Alabama. The transverse distribution of the wheel loads and two-dimensional behavior of the bridge were considered, and different girders were assumed to have different

properties, so that each girder had its own IL. Further, Moses' algorithm (Moses 1979) was modified to include the transverse distribution of wheel loads, and a method was presented to calculate the axle weights based on the calculated ILs of each girder. Mathematical equations to calculate the ILs and axle weights were derived, and the proposed algorithms were implemented by a computer program in MATLAB. Field testing of a concrete slab-girder bridge on highway US-78 was carried out to evaluate the accuracy of the proposed algorithm in identifying axle weights, with the comparison of static weights and with results from a bending-plate WIM (BPWIM) system for assessment of moving heavy vehicles.

BWIM System for Case Study

The main parts of the BWIM system include: (1) weighing sensors and FAD sensors to acquire signals; (2) an antenna, a personal digital assistant (PDA), and a wireless fidelity (Wi-Fi) system allowing communication through the transmission control protocol/internet protocol (TCP/IP); (3) a camera system to recognize and capture pictures of vehicles; and (4) solar panels and batteries to provide power. The components of the BWIM system installed in the case-study bridge are illustrated in Fig. 1.

(1) FAD sensors; (2) spider (to connect sensors to be easily connected to the cabinet); (3) weighing sensors; (4) cabinet & panel; (5) housing for batteries; (6) solar panels; (7) solar panel installation; (8) antenna; (9) camera; (10) PDA

Fig. 1 Components of the BWIM system

The bridge selected for the application of the BWIM system is located on highway US-78 East in Graysville, Alabama, three miles west of I-22. The number of the bridge is BIN 7633. The reason of choosing the bridge for field testing is that it is a simple supported concrete slab-girder bridge, a typical type of bridge in Alabama and other states in the U.S. In addition, located approximately four miles to the west of the instrumented bridge is an Alabama Department of Transportation (ALDOT)-operated bending plate WIM (BPWIM) system, which is one of ALDOT's eleven pavement WIM sites. This allows evaluation of the performance of the BWIM system by comparing with the static weights of trucks and with the weight measurements of the BPWIM system. Thus, the relative accuracy of all three weighing systems can be assessed under the same testing conditions.

The bridge has two identical south and north parts. Each part is composed of three simple supported T-beams with spans of 3×42 ft (12.8m) $= 126$ ft (38.4 m) and with two lanes in the same direction. The south part was selected for the field test. The bridge is smooth on the joints, and the approach to the bridge is even.

In identifying axle weights and GVW of moving vehicles with the BWIM system, bridges with smoother approaches without bumps before the instrumented span will give more accurate results. When vehicles pass the instrumented bridge, they bounce on their tires and suspensions. Usually, this motion includes: (1) low frequency vertical bouncing of the sprung masses and; (2) high frequency bouncing of the axles (wheel hop). The magnitude of the bounce depends on the roughness of the road profile, the type of suspension and the vehicle's speed. When there is no major unevenness (e.g., bumps, ruts, potholes in the pavement, faulty expansion joints) on the approach to or on the instrumented bridge, the level of dynamics is generally low. Hence, to improve the accuracy in identifying axle weights and GVW, the selected bridge span should have smooth approaches and even road surfaces. In addition, the bridge instrumented for BWIM should have higher eigen-frequencies to avoid the matching of vehicle bouncing and hopping frequencies with the bridge first natural frequency and other pseudo-frequencies associated with axle spacings. In practice this can be achieved by selecting a short span bridge for BWIM.

Fig. 2 shows the sensor positions on the bridge, and Fig. 3 illustrates the cross section of the exterior and interior girders. The end span in the east direction was selected as the test span for applying the BWIM system (Fig. 2). Four weighing sensors were mounted longitudinally on the soffits of concrete girders (one sensor for each girder), 30.5 cm (1 ft) off the center because of the diaphragm. To detect vehicles and acquire the number of axles, axle spacing, and speed for each vehicle separately, four FAD sensors were mounted longitudinally, 365.8 cm (12 ft) apart, underneath the concrete slab.

Initial Calibration of the BWIM System

The initial calibration was carried out under test condition (R1-I) according to the European specifications for WIM (COST 323, 1999). In COST 323, four different test conditions and three different environmental conditions are used. The test conditions are (1) full repeatability (r1); (2) limited repeatability (r2); (3) limited reproducibility (R1), and (4) full reproducibility (R2). For test conditions (1) and (2), only one vehicle with repeated runs is required. The difference is that the former is under the same loading and traffic conditions, whereas the latter is under different conditions. R1 requires from two to ten trucks driven at several times under changing traffic conditions, but R2 requires more than ten vehicles to form a traffic flow. The environmental conditions are (1) environmental repeatability (I), representing short measurements in mostly constant environmental conditions - weather; (2) environmental limited reproducibility (II), representing short measurements in changing environmental conditions - weather; and (3) environmental full reproducibility (III), representing long-term measurements in changing environmental conditions - weather (ZAG, 2005). It was observed that the representative vehicle for US-78 highway was a semi-trailer, so the initial calibration was conducted with two pre-weighed semi-trailers, provided by ALDOT and loaded to their capacity of 80,000 lbs (36,287kg). The details of the calibration vehicles are listed in Table 1. It is acknowledged that this is a very limited range of truck types. However, the main purpose of calibration is to find the influence line which characterizes the response of the bridge to a unit axle load so the result is not sensitive to truck type.

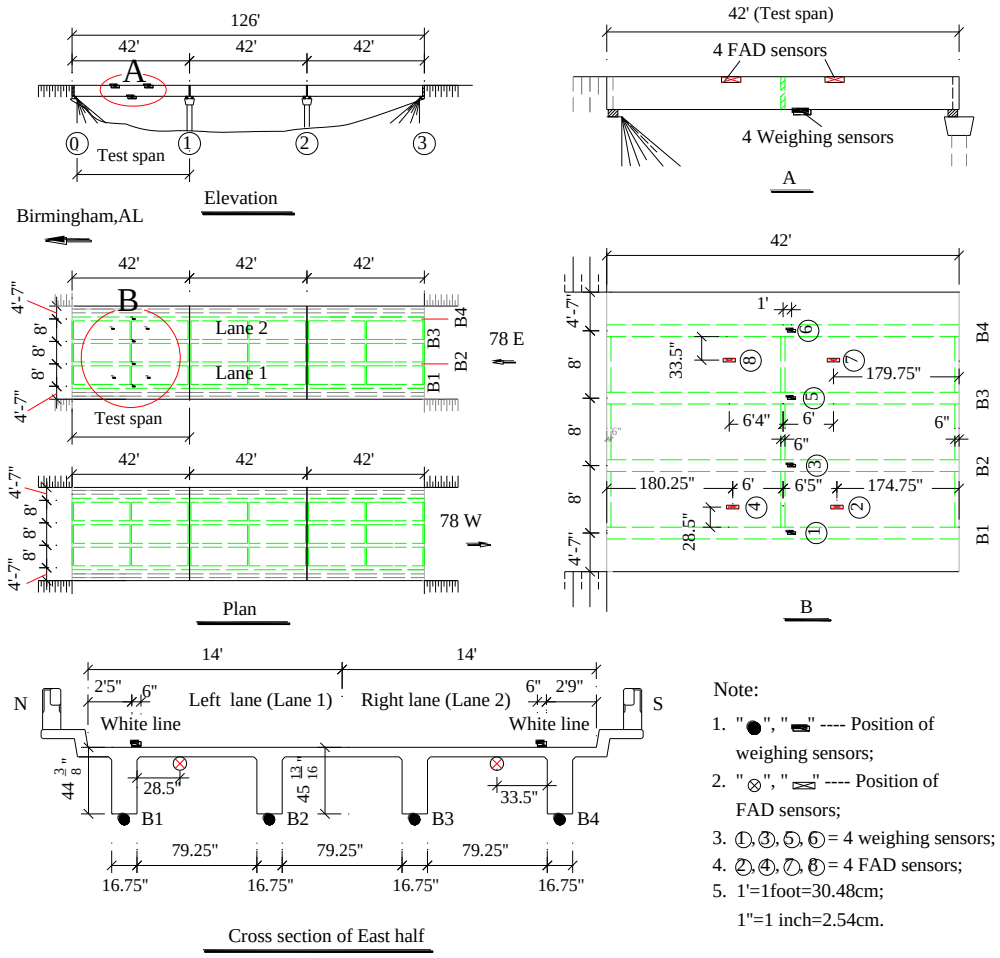

Fig. 2 Sensor positions

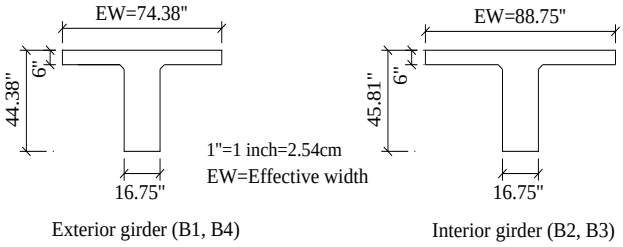

Fig. 3 Cross section of exterior and interior girders

Table 1. Vehicle information for the initial calibration

Vehicle No.	Axle weight (lb)						Axle distance (inches)			
	GVW	1st axle	2nd axle	3rd axle	4th axle	5th axle	A1-A2	A2-A3	A3-A4	A4-A5
1	79,000	11,050	15,650	16,100	18,200	18,000	170	53	440	51
2	78,200	10,050	16,000	15,800	18,300	18,050	171	53	438	50

Note: 1 lb= 0.454 kg, 1 inch=2.54 cm

During the initial calibration test, the two calibration vehicles ran repeatedly at different speeds on different lanes. There were ten runs for each lane. To verify the proposed algorithm in IL calculations and axle weight identification, ten repeated runs on Lane 1 and Lane 2 were selected as reference. Fig. 4 shows pictures of the calibration vehicles.

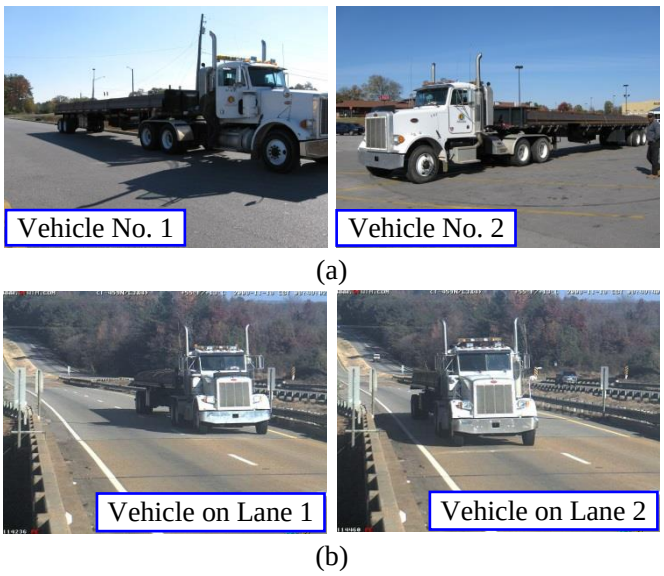

Fig. 4 Vehicles for the initial calibration of bridge on US-78 highway: (a) Static photo; (b) Photo captured from the BWIM system

Determination of Axle Spacing and Number of Axles

The BWIM system introduced here is a FAD BWIM system. The FAD sensors were mounted on the underside of the bridge slab to detect vehicles and acquire the number of axles, axle spacing, and speed for each vehicle. Figs. 5 and 6 show the signals recorded by eight sensors (four weighing sensors and four FAD sensors) when calibration vehicle 1 passed the instrumented bridge on Lane 1. In Fig. 5, B1, B2, B3, and B4 represent the signals obtained by four weighing sensors mounted on the soffit of each girder – note that there are no individual peaks corresponding to each axle. Fig. 6 shows the signals acquired from four FAD sensors with the vehicle passing across the bridge along Lane 1. In these figures, L1-FAD-1 and L1-FAD-2 represent the FAD sensors of Lane 1, and the vehicle passed L1-FAD-1 first and then L1-FAD-2. Similarly, L2-FAD-1 and L2-FAD-2 represent the FAD sensors of Lane 2, and the vehicle passed L2-FAD-1 first and then L2-FAD-2.

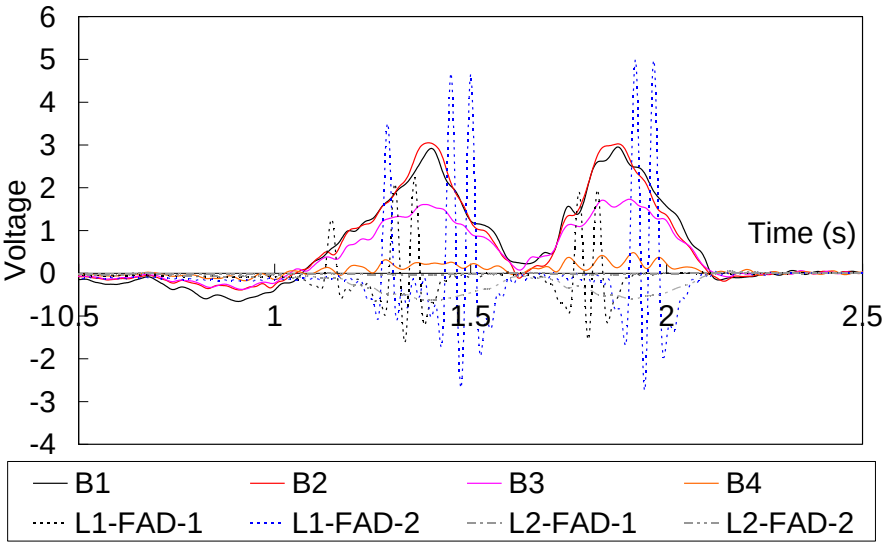

Fig. 5 Signals recorded by weighing sensors and FAD sensors

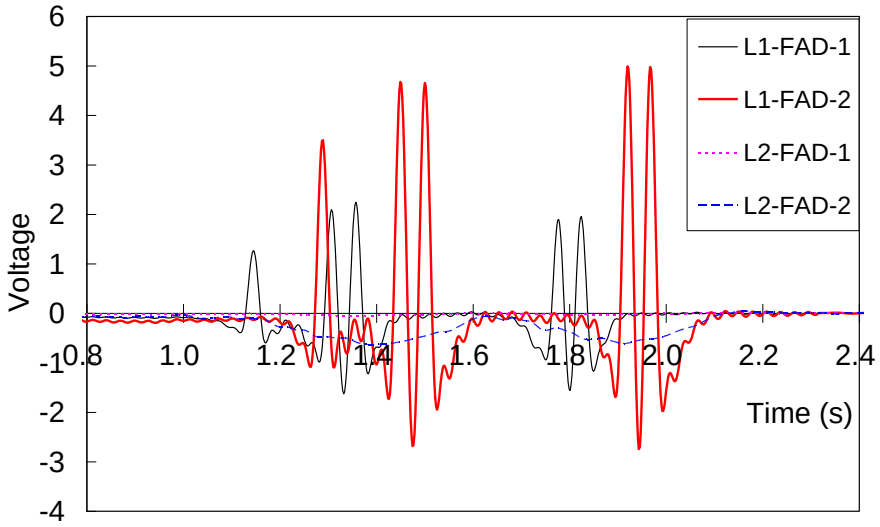

Fig. 6 Signals acquired from four FAD sensors with vehicle passing across Lane 1

Since the FAD sensors were mounted right underneath the slab, their signals had clear peaks when the axle passed the sensor position. As can be seen from Fig. 6, when the calibration vehicle (5-axle semitrailer) passed the bridge, the two FAD sensors of Lane 1 were activated and the signals of these two FAD sensors had five peaks, while no peak was observed for the signals of the two FAD sensors of Lane 2. The peaks occurred at the very time when the axle passed over the FAD sensors. From Fig. 6, one would know that the truck crossing the bridge was on Lane 1, and the truck was 5-axle since both L1-FAD-1 and L1-FAD-2 had five peaks. Additionally, taking the signals of L1-FAD-1 as an example, the first peak was separated from other four peaks, and one thus can identify this as a single axle; since the second and the third peaks were closely spaced and were separated from the other three peaks, one can identify these two peaks as a closely-spaced group of axles; similarly, the fourth and the fifth peaks can also be identified as another closely-spaced group of axles. From this case, one would know that the 5-axle truck was composed of one single axle and two closely-spaced groups of axles. The signals of L1-FAD-2 also demonstrate this and can be used to accurately calculate the speed.

The time instants (taking the starting time of recording as 0) corresponding to the five peaks of L1-FAD-1 are taken as t_1, t_2, t_3, t_4, and t_5, respectively; and the five counterparts for L1-FAD-2 are t_1', t_2', t_3', t_4', and t_5', respectively. Provided the calibration vehicle passed the bridge at a constant speed, v, and the distance of the two FAD sensors along the driving direction is taken to be L_{FAD}, which was measured before the calibration test, the vehicle speed, v, can be calculated as

$$v = L_{FAD}/(t_i' - t_i) \qquad (i = 1, 2, 3, 4, 5) \tag{1}$$

The axle spacing between the i^{th} and $(i+1)^{th}$ axles ($(i = 1, 2, 3, 4)$ for the 5-axle semi-trailer), $A_{i,i+1}$, can be calculated as

$$A_{i,i+1} = v \cdot (t_{i+1} - t_i) \qquad (i = 1, 2, 3, 4) \tag{2}$$

$$\text{or} \quad A_{i,i+1} = v \cdot (t_{i+1}' - t_i') \quad (i = 1, 2, 3, 4) \tag{3}$$

When taking the first run on Lane 1 as an example, the time instants of the five peaks of L1-FAD-1 corresponded to $t_1 = 1.148s$, $t_2 = 1.309s$, $t_3 = 1.361s$, $t_4 = 1.779s$, and $t_5 = 1.828s$, respectively; the time instants of the five peaks of L1-FAD-2 were $t_1' = 1.293s$, $t_2' = 1.453s$, $t_3' = 1.506s$, $t_4' = 1.924s$,

and t_5'$=1.973s$. The time lag for the first axle between the corresponding peaks of the two FAD sensors was t_1'$-t_1=0.145s$. Similarly, one can obtain the other four time lags as t_2'$-t_2=0.145s$, t_3'$-t_3=0.145s$, t_4'$-t_4=0.145s$, and t_5'$-t_5=0.145s$. As can be seen from Fig. 2, $L_{FAD}=3.79m$. Then the vehicle velocity was calculated as $v=26.223m/s$. Taking the signal of L1-FAD-1 as an example, one knew that when the 5-axle vehicle passed the FAD sensors, the time lag between the first and second axles was $t_2-t_1=0.160s$, and then one obtained the axle spacing, $A_{1,2}=4.200m(165.3ft)$. Similarly, one can obtain the other three axle spacings as, $A_{2,3}=1.383m(54.4ft)$, $A_{3,4}=10.960m(431.5ft)$, and $A_{4,5}=1.280m(50.4ft)$, respectively.

Table 2 illustrates the percentage errors of the identified axle spacings from 10 runs on Lane 1, compared with the static measurements. The identified vehicle speeds are also listed in this table.

Table 2. Errors in axle spacings and calculated vehicle speeds

Item	Lane	Axle spacing	run 1	run 2	run 3	run 4	run 5	run 6	run 7	run 8	run 9	run 10
Percentage error of identified axle spacing (%)	Lane 1	A1-A2	-2.7	-2.5	-2.6	-1.4	-1.6	-3.7	-2.4	-3.3	-3.3	-2.0
		A2-A3	2.7	5.6	4.1	0.3	2.7	2.4	0.0	2.7	5.2	4.1
		A3-A4	-1.9	-0.6	-2.0	-2.0	-1.9	-2.2	-1.4	-1.9	-1.9	-1.1
		A4-A5	-1.2	-2.5	0.2	0.2	-1.2	4.6	2.1	4.9	4.3	6.3
	Lane 2	A1-A2	-0.7	-0.6	2.4	0.1	-0.7	2.0	17.6	0.8	1.4	0.6
		A2-A3	8.0	9.5	6.2	8.8	6.2	11.7	8.2	7.7	7.7	6.2
		A3-A4	0.5	0.9	2.3	1.0	-0.5	1.9	-18.8	1.4	2.4	1.4
		A4-A5	10.5	12.0	8.4	11.5	6.3	7.8	135.8	3.7	5.7	6.3
Identified vehicle speed (m/s)	Lane 1		26.22	26.95	26.58	26.58	26.22	25.20	25.53	26.22	23.38	26.58
	Lane 2		25.67	26.02	27.11	25.00	27.11	27.50	24.06	27.50	27.50	27.11

IL Calculation Considering Transverse Wheel Load Distribution

In calculating axle weights, an IL based on actual strain readings acquired at the site can represent the bridge behavior in the algorithm of the BWIM system, providing more accuracy, especially for the identification of axle weights, because they are redistributed in the case of poor ILs (McNulty and O'Brien, 2003; ZAG, 2005). In the algorithm presented here, each girder of the bridge was deemed to have separate properties (the modulus of elasticity, E, and the section modulus, Z), and the transverse distribution of wheel loads was included. Based on repeated runs of the calibration trucks, the field-calibrated ILs of different girders were calculated.

Calculation of Wheel Load Distribution of Different Girders

Fig. 7 illustrates the case when a calibration truck with N known axle weights, P_1, P_2, $\cdots$, P_N, passed the bridge. In order to simulate the bridge as a two-dimensional structure, the wheel load distribution along the transverse direction of the bridge was considered; then the distributed load of the wheels acting on each girder could be calculated. Although there are various methods to calculate the theoretical load distribution of wheel loads, in the present research, the actual measured strain data was applied to account for the wheel load distribution of each girder with vehicles passing across the instrumented bridge.

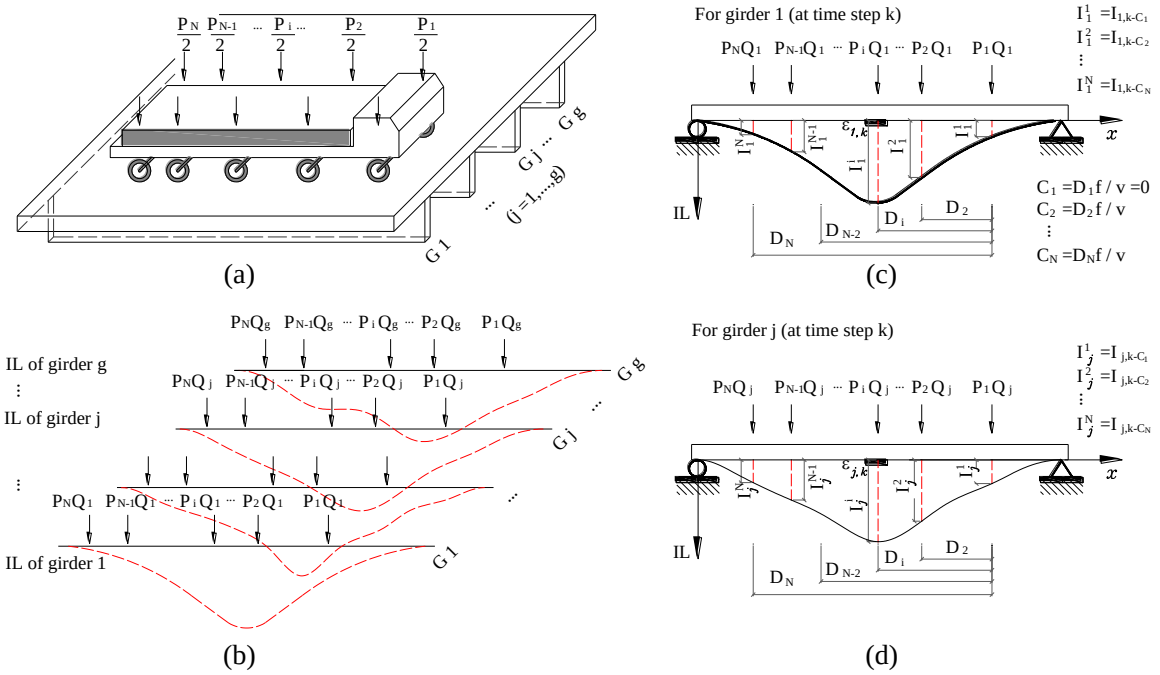

Fig. 7 IL ordinates of different girders: (a) Calibration vehicle crossing the bridge; (b) Distributed axle loads acting on different girders; (c) Distributed axle loads acting on the 1st girder; (c) Distributed axle loads acting on the jth girder

In introducing the transverse load distribution to the algorithm, the following was noted. The AASHTO (2012) specification demonstrates that the transverse load distribution factors are slightly different for bending moment and shear force. Moreover, along the driving direction, the transverse load distribution factor of each girder is position-dependent due to many factors, such as transverse connectivity between longitudinal members at mid-span and support. However, most slab-girder bridges, have equally distributed lateral connectivity in the vicinity of mid-span. It is therefore feasible to consider the lateral load distribution factors as unchanged in the large range around mid-span. Consideration of all the different parts of bridges having different transverse load distribution factors for each girder would be more accurate, but it would increase run-time and would require a more complex calibration process. Hence, for simplicity and real time implementation, the dynamic response of the mid part was thus selected as a reference to acquire the transverse load distribution factors of each girder.

Based on the continuous data recorded during the process of the vehicle passing over the bridge, the maximum peak strains for all the girders could be found. From the time instant when the first axle reached the position prior to the bridge (the starting-point for the IL) to the time instant when the last axle left the position posterior to the bridge, there were total K scans of the strain data (from time step 1 to K). Among the recording data for a reference girder that appeared maximum peak strain, the largest 50 strains were selected, and the corresponding strains for other girders could be found similarly. For example, the maximum peak strain was located at the jth girder at time step k (the strain is recorded as $\varepsilon_{j,k}$, k = 1 … K), and the corresponding strains for other girders at time step k were recorded as $\varepsilon_{1,k}, \varepsilon_{2,k}, \cdots, \varepsilon_{j-1,k}, \varepsilon_{j+1,k}, \cdots, \varepsilon_{g,k}$ (the number of girders is g). Then the transverse load distribution factor of wheel load for the jth girder at time step k was expressed as

$$Q_{j,k} = \frac{\varepsilon_{j,k}}{\sum_{j=1}^{g} \varepsilon_{j,k}} \quad (j = 1, \cdots, g) \tag{4}$$

According to the measured bridge response, Eq. (4) could be followed for selecting the largest 50 strains and their corresponding time instants to calculate $Q_{j,k}$ and the average was further conducted to obtain the transverse load distribution factors of the wheel loads, $Q_1, Q_2, \cdots, Q_g$, for the g girders. For the repeated ten runs along Lanes 1 and 2, ten transverse load distribution factors of wheel loads could be obtained for each girder, given in Table 3. The corresponding loads acting on each girder due to wheel loads are listed in Table 4.

Table 3. Load distribution factor for each girder under repeated runs

	Lane 1				Lane 2			
	Q_1	Q_2	Q_3	Q_4	Q_1	Q_2	Q_3	Q_4
run 1	0.3673	0.3933	0.2094	0.0300	0.0869	0.2258	0.4315	0.2558
run 2	0.3887	0.3872	0.1963	0.0279	0.0842	0.2209	0.4311	0.2638
run 3	0.3885	0.3863	0.1990	0.0262	0.0708	0.1892	0.4261	0.3140
run 4	0.3162	0.4071	0.2326	0.0441	0.0744	0.2066	0.4314	0.2876
run 5	0.3654	0.3969	0.2036	0.0341	0.1007	0.2498	0.426	0.2235
run 6	0.3506	0.4089	0.2108	0.0297	0.0924	0.2398	0.4317	0.2361
run 7	0.3933	0.3830	0.1948	0.0289	0.0929	0.2224	0.4211	0.2635
run 8	0.3463	0.4110	0.2107	0.0320	0.0707	0.2002	0.4306	0.2984
run 9	0.3791	0.4040	0.1911	0.0258	0.0702	0.2142	0.426	0.2896
run 10	0.3357	0.4103	0.2199	0.0341	0.0760	0.2095	0.4311	0.2835
Average	0.3631	0.3988	0.2068	0.0313	0.0819	0.2178	0.4287	0.2716

Table 4. Wheel load effect on each girder

Axle \ Girder	1#	2#	⋯	g#
1st axle	$P_1 \times Q_1$	$P_1 \times Q_2$	⋯	$P_1 \times Q_g$
2nd axle	$P_2 \times Q_1$	$P_2 \times Q_2$	⋯	$P_2 \times Q_g$
⋮	⋮	⋮	⋮	⋮
Nth axle	$P_N \times Q_1$	$P_N \times Q_2$	⋯	$P_N \times Q_g$

Calculation of ILs of Different Girders

In the calculations, it was assumed that, after the wheel loads were distributed on each girder according to obtained transverse load distribution factors, each girder only carried the distributed portion by itself.

With the calibration vehicles passing over the instrumented bridge, the bridge response (strain) was measured continuously and recorded at a high rate of sampling (512 Hz). In this manner, the theoretical bridge response (strain) could be predicted. The algorithm for IL calculation was based on the least-square method with minimizing the difference between the measured and predicted responses (strains) at mid-span. To differentiate the defined error function with respect to each IL coordinate, a set of simultaneous equations was established, and the coordinates of IL were calculated correspondingly.

For a static distributed load at a certain location on the *j*th girder, the longitudinal gross bending moment at a specific bridge section (mid span) at time step k could be expressed as a function of time. At time step k, the bending moment of the *j*th girder, M_k^j, was derived:

$$M_k^j = E_j Z_j \varepsilon_{j,k}^t \tag{5}$$

where M_k^j is the bending moment of the *j*th girder; Z_j and E_j were the section modulus and the modulus of elasticity of the *j*th girder, respectively; and $\varepsilon_{j,k}^t$ was the predicted strain at time step k at the soffit of the *j*th girder.

For the calibrations, vehicle velocity was assumed to be constant, to be determined according to the two FAD sensors mounted under the slab of the bridge near $L/4$ and $3L/4$ (see Fig. 2 and Fig. 6).

When a calibration truck with N known axle weights, P_1, P_2, ..., P_N, passed over the bridge (see Fig. 7), at time step k, the corresponding theoretical load effect caused by the distributed load was

$$M_k^j = \sum_{i=1}^{N} P_i Q_j I_{j,(k-C_i)} \tag{6}$$

where $P_i Q_j$ was the distributed load to the *j*th girder by axle load P_i ($i = 1, \cdots, N$), and $I_{j,(k-C_i)}$ was the corresponding IL coordinate of the distributed load to the *j*th girder.

The corresponding theoretical bridge response (theoretical strain, $\varepsilon_{j,k}^t$, for the *j*th girder) caused by the calibration truck at time step k was

$$M_k^j = E_j Z_j \varepsilon_{j,k}^t = \sum_{i=1}^{N} P_i Q_j I_{j,(k-C_i)} \tag{7}$$

Then one obtained

$$\varepsilon_{j,k}^t = \frac{1}{E_j Z_j} \sum_{i=1}^{N} P_i Q_j I_{j,(k-C_i)} \tag{8}$$

$$C_i = \frac{D_i f}{v} \tag{9}$$

where f is the scanning frequency of a sampling system with a high rate of data acquisition; v denotes the vehicle velocity; D_i represents the distance between the ith and the first axles; and C_i stands for the number of scans corresponding to D_i ($C_1 = 0$). The details are illustrated in Fig. 7.

Since there was no need to know the exact position at which the applied load caused the bridge to start bending, the uncertainty about the real boundary conditions and the small strains generally induced near the supports were ignored (González and O'Brien, 2002). Based on the least-square method, an error function for the *j*th girder between the measured bridge response of the *j*th girder and the theoretical one was defined as

$$E = \sum_{k=1}^{K} (\varepsilon_{j,k}^m - \varepsilon_{j,k}^t)^2 \tag{10}$$

where $\varepsilon_{j,k}^m$ was the measured strain at the *j*th girder at time step k.

For simplification, a three-axle calibration truck was used as an illustrative example to derive IL coordinates. In this case, the theoretical bridge response (strain) under the truck at time step k was

$$\varepsilon_{j,k}^t = \frac{1}{E_j Z_j} [(P_1 Q_j I_{j,(k-C_1)} + P_2 Q_j I_{j,(k-C_2)} + P_3 Q_j I_{j,(k-C_3)})] \qquad k = 1, \cdots, K \tag{11}$$

The error function could be expanded as:

$$E = (\varepsilon_{j,1}^m - \varepsilon_{j,1}^t)^2 + \ldots + (\varepsilon_{j,R}^m - \varepsilon_{j,R}^t)^2 + \ldots + (\varepsilon_{j,R+C_2}^m - \varepsilon_{j,R+C_2}^t)^2 + \ldots + (\varepsilon_{j,R+C_3}^m - \varepsilon_{j,R+C_3}^t)^2 + \ldots + (\varepsilon_{j,K}^m - \varepsilon_{j,K}^t)^2 \tag{12}$$

In the error function, items relating to $I_{j,R}$ ($R = 1, \cdots, K - C_3$) were $\varepsilon_{j,R}^t$, $\varepsilon_{j,R+C_2}^t$, and $\varepsilon_{j,R+C_3}^t$. Differentiating E with respect to the set of IL coordinates of the *j*th girder, $I_{j,R}$, yielded

$$\begin{aligned}\partial E/\partial I_{j,R} &= 2\{[1/(E_jZ_j)]\varepsilon^m_{j,R} - [1/(E_jZ_j)^2](P_1Q_jI_{j,R} + P_2Q_jI_{j,(R-C_2)} + P_3Q_jI_{j,(R-C_3)})\}(-P_1Q_j)\\ &+ 2\{[[1/(E_jZ_j)]\varepsilon^m_{j,R+C_2} - [1/(E_jZ_j)^2](P_1Q_jI_{j,(R+C_2)} + P_2Q_jI_{j,R} + P_3Q_jI_{j,(R+C_2-C_3)})\}(-P_2Q_j)\\ &+ 2\{[1/(E_jZ_j)]\varepsilon^m_{j,R+C3} - [1/(E_jZ_j)^2](P_1Q_jI_{j,(R+C_3)} + P_2Q_jI_{j,(R+C_3-C_2)} + P_3Q_jI_{j,R})\}(-P_3Q_j)\end{aligned} \quad (13)$$

To minimize E, the set of IL coordinates made the partial derivatives zero.

$$\partial E/\partial I_{j,R} = 0 \qquad (R = 1, \cdots, K - C_3) \quad (14)$$

Summing the above $K - C_3$ equations from time step $R = 1, \cdots, K - C_3$, the equations could be written in a matrix form as:

$$[W]_{(K-C_3)\times(K-C_3)} \times \{I_j\}_{(K-C_3)\times 1} = \{\varepsilon_j\}_{(K-C_3)\times 1} \quad (15)$$

where $\{I_j\}$ denoted an IL coordinate vector of the *j*th girder; $\{\varepsilon_j\}$ was a vector dependent on the axle weights of the vehicle and the measured response (strain) of the first girder, the element of the vector at row R was $\varepsilon_{j,R} = E_jZ_j(P_1Q_j\varepsilon^m_{j,R} + P_2Q_j\varepsilon^m_{j,R+C_2} + P_3Q_j\varepsilon^m_{j,R+C3})$ $(R = 1, \cdots, K - C_3)$; and $[W]$ was a sparse symmetric matrix dependent on the distributed load acting on the first girder listed as follows:

$$[W]_{(K-C_3)\times(K-C_3)} =$$

$$\begin{bmatrix}
W_{R,R} & \cdots & \cdots & W_{R,(R+C_2-C_1)} & \cdots & W_{R,(R+C_3-C_2)} & \cdots & W_{R,(R+C_3-C_1)} & & & & \\
 & \ddots & \cdots & \cdots & \ddots & & \ddots & \cdots & \ddots & & 0 & \\
 & \cdots & W_{R,R} & \cdots & \cdots & W_{R,(R+C_2-C_1)} & \cdots & W_{R,(R+C_3-C_2)} & \cdots & W_{R,(R+C_3-C_1)} & & \\
 & & \cdots & W_{R,R} & \cdots & \cdots & W_{R,(R+C_2-C_1)} & \cdots & W_{R,(R+C_3-C_2)} & \cdots & W_{R,(R+C_3-C_1)} & \\
 & & & & \ddots & \cdots & \cdots & \ddots & \cdots & \ddots & \cdots & \ddots \\
 & & & & & W_{R,R} & \cdots & \cdots & W_{R,(R+C_2-C_1)} & \cdots & W_{R,(R+C_3-C_2)} & \cdots \\
 & & & & & & \ddots & \cdots & \cdots & \ddots & \cdots & \ddots \\
 & & & & & & & W_{R,R} & \cdots & \cdots & W_{R,(R+C_2-C_1)} & \cdots \\
 & & & & & \textit{Symmetric} & & & W_{R,R} & \cdots & \cdots & W_{R,(R+C_2-C_1)} \\
 & & & & & & & & & \ddots & \cdots & \cdots \\
 & & & & & & & & & & W_{R,R} & \cdots \\
 & & & & & & & & & & & W_{R,R}
\end{bmatrix} \quad (16)$$

From matrix $[W]$, the main diagonal was the sum of the squares of distributed axle weights. In each row of the matrix, the numbers of off-diagonals which lay in the distances (between each of the two axles) from the main diagonal was the product of distributed weight of these two axles. For example, in the distances $C_2 - C_1$, $C_3 - C_2$, and $C_3 - C_1$ ($C_1 = 0$), these numbers were $(P_2Q_j)(P_1Q_j)$, $(P_3Q_j)(P_2Q_j)$, and $(P_3Q_j)(P_1Q_j)$, respectively. Similarly, in the positions $C_1 - C_2$, $C_2 - C_3$, and $C_1 - C_3$, these numbers were $(P_1Q_j)(P_2Q_j)$, $(P_2Q_j)(P_3Q_j)$, and $(P_1Q_j)(P_3Q_j)$, respectively. The other numbers in this row were zeros. For a three-axle calibration vehicle, the main diagonal was

$$W_{R,R} = \sum_{i=1}^{3}(P_iQ_j)^2 = (P_1Q_j)^2 + (P_2Q_j)^2 + (P_3Q_j)^2 \qquad (R = 1, \cdots, K - C_3) \quad (17)$$

The upper triangle elements were

$$\begin{aligned}
&W_{R,R+(C_3-C_2)} = (P_2Q_j)(P_3Q_j); && R + (C_3 - C_2) \le K - C_3\\
&W_{R,R+(C_2-C_1)} = (P_1Q_j)(P_2Q_j); && R + C_2 \le K - C_3\\
&W_{R,R+(C_3-C_1)} = (P_1Q_j)(P_3Q_j); && R + C_3 \le K - C_3
\end{aligned} \quad (18)$$

The other numbers in this matrix were zeros, and the corresponding lower triangular elements were symmetric. For the calibration vehicle passing over the bridge, the IL coordinates of the *j*th girder were calculated as:

$$\{I_j\}_{(K-C_3)\times 1} = [W]^{-1}{}_{(K-C_3)\times(K-C_3)} \times \{\varepsilon_j\}_{(K-C_3)\times 1} \quad (19)$$

The above equations were exclusively for three-axle vehicles, but, for vehicles with different numbers of axles, similar equations could be derived. If the calibration vehicle had N axles, the matrix equation would be:

$$[W]_{(K-C_N)\times(K-C_N)} \times \{I_j\}_{(K-C_N)\times 1} = \{\varepsilon_j\}_{(K-C_N)\times 1} \tag{20}$$

$$\{I_j\}_{(K-C_N)\times 1} = [W]^{-1}{}_{(K-C_N)\times(K-C_N)} \times \{\varepsilon_j\}_{(K-C_N)\times 1} \tag{21}$$

where $\{\varepsilon_j\}$ in Eq. (21) was similar to that in Eq. (15); the element of the vector at row R was $\varepsilon_{j,R} = E_j Z_j (P_1 Q_j \varepsilon^m_{j,R} + P_2 Q_j \varepsilon^m_{j,R+C_2} + P_3 Q_j \varepsilon^m_{j,R+C3} + \cdots P_N Q_j \varepsilon^m_{j,R+C_N})$ $(R = 1, \cdots, K - C_3)$; and the elements of matrix $[W]$ were as follows:

$$W_{R,R} = \sum_{i=1}^{N} (P_i Q_j)^2 = (P_1 Q_j)^2 + (P_2 Q_j)^2 + \cdots + (P_N Q_j)^2 \qquad R = 1, \cdots, K - C_N \tag{22}$$

$$W_{R,R+(C_s - C_t)} = (P_s Q_j)(P_t Q_j); \qquad R + (C_s - C_t) \le K - C_3$$
$$R = 1, \cdots, K - C_N; \quad s > t; \quad s = 1, \cdots, N; \quad t = 1, \cdots, N; \tag{23}$$

Then the IL coordinates of the jth girder were calculated as, $\{I_j\}_{(K-C_N)\times 1}$, with the calibration vehicle crossing the bridge. Similarly, the IL coordinates of other girders could be calculated, as $\{I_1\}_{(K-C_N)\times 1}, \{I_2\}_{(K-C_N)\times 1}$, $\cdots, \{I_{j-1}\}_{(K-C_N)\times 1}, \{I_{j+1}\}_{(K-C_N)\times 1}, \cdots, \{I_g\}_{(K-C_N)\times 1}$. From this method, different ILs of each girder could be acquired with the calibration vehicles passing over the instrumented bridge, considering the transverse distribution of wheel loads to take into account the two-dimensional behavior of the bridge.

Comparison of the predicted bridge responses based on calculated ILs with measured bridge responses

Based on the proposed algorithm for calculation of ILs considering the transverse wheel load distribution, with the ten runs of calibration vehicles on the same lane (Lane 1 of bridge on US-78 highway), ten different ILs for each girder could be obtained. The ILs of each girder for run 1 (on Lane 1) are listed in Fig. 8 along with theoretical IL. A comparison of the measured and predicted bridge response of each girder is shown in Fig. 9.

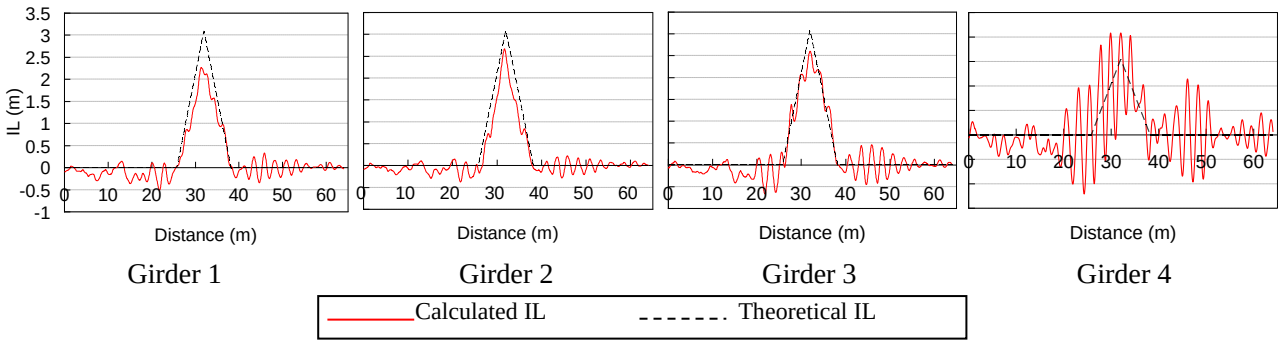

Fig. 8 The calculated and theoretical ILs of girders based on the first run (vehicle in Lane 1)

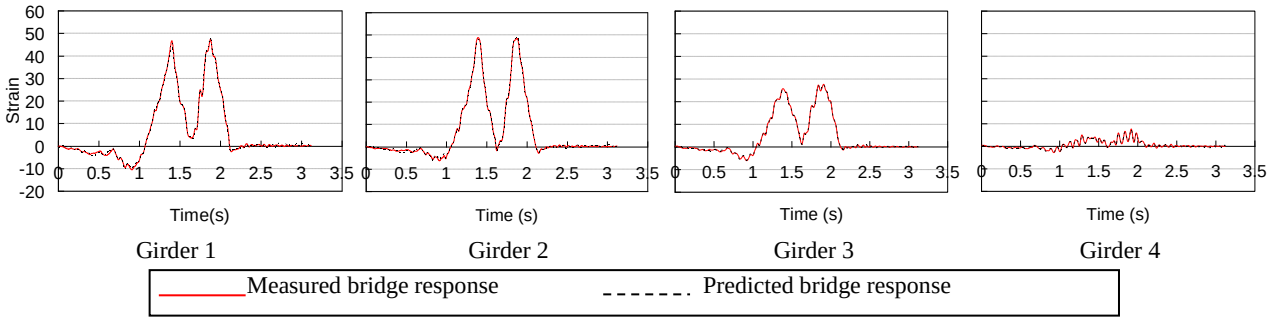

Fig. 9 The measured and predicted response based on the first run (vehicle in Lane 1)

From the cross section shown in Fig. 2, it was evident that, when the vehicle was in Lane 1, the wheel loads were mainly carried by girders 1 and 2; and when the vehicle was in Lane 2, the wheel loads were mainly carried by girders 3 and 4. The measurements of strain confirmed this. Even if the ILs of all girders could be calculated from each run in each lane, the values would not be accurate for girders far from the vehicle. For example, when the vehicle was in Lane 1, the ILs of girders 3 and 4, which were illustrated in Fig. 8, were not accurate, especially that for girder 4. Thus, the ILs for girders 3 and 4 would be more accurate if they were calculated based on the bridge response when the vehicle was in Lane 2. With run 2 in Lane 2 as an example, the ILs of each girder are listed in Fig. 10. A comparison of the measured and predicted bridge responses of each girder is illustrated in Fig. 11. The agreement between the measured and predicted bridge responses of all girders demonstrates the effectiveness and accuracy of the proposed algorithm in the calibration of ILs of each girder. However, the proposed method has some limitations that become evident during the process of obtaining the IL for each girder based on the measured data: (1) The calibration vehicle should be heavy enough to instigate a sufficiently large response; (2) The effect of strong vibrations needs to be clarified quantitatively and may be a problem in more flexible bridges; and (3) The proposed method is useful for multiple T/I girder and solid slab bridges, and can also be applicable for orthotropic steel deck bridges. Currently, the methodology is not suitable for longer spans such as box-girder bridges.

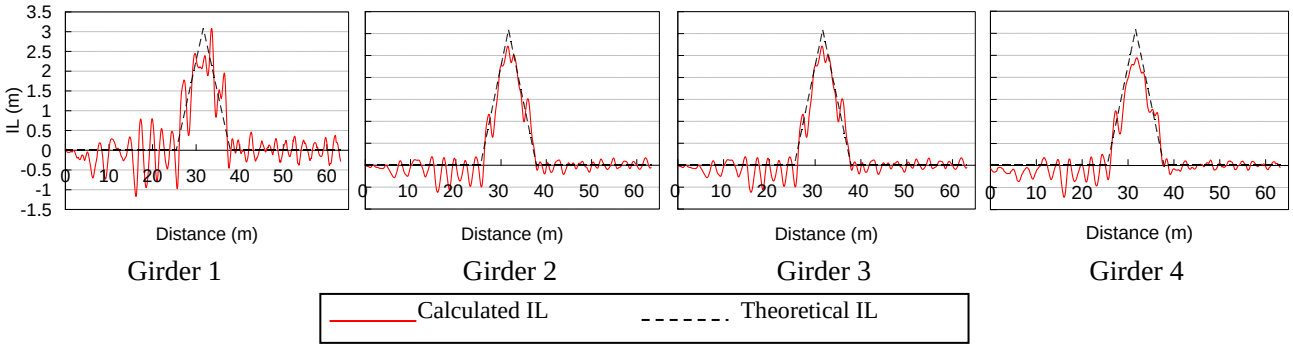

Fig. 10 The calculated IL of all girders (vehicle in Lane 2)

From Figs 8, 9, 10 and 11, we concluded that the ILs of girders 1 and 2 should be based on the bridge response of repeated runs in Lane 1, and the ILs of girders 3 and 4 should be based on those for Lane 2. First, the ILs from the repeated runs in Lanes 1 and 2 were calculated, and then the calculated ILs from the repeated runs in each lane were summed to obtain the average ILs for each girder as references for the calculation of axle weights. For girders 1 and 2, seven repeated runs (without runs 3, 7, and 10) were selected for averaging; for girders 3 and 4, eight repeated runs (without runs 5 and 7) were selected for averaging. Fig. 12 shows the averaged ILs of each girder.

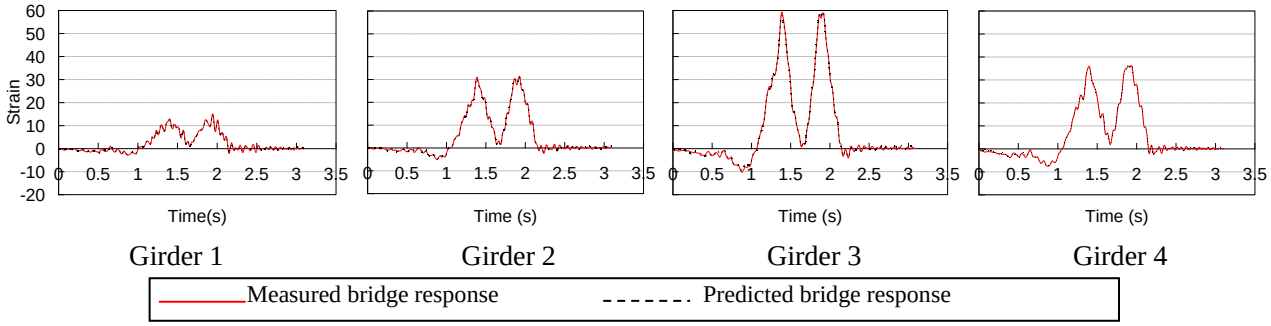

Fig. 11 The measured and predicted responses of all girders (vehicle in Lane 2)

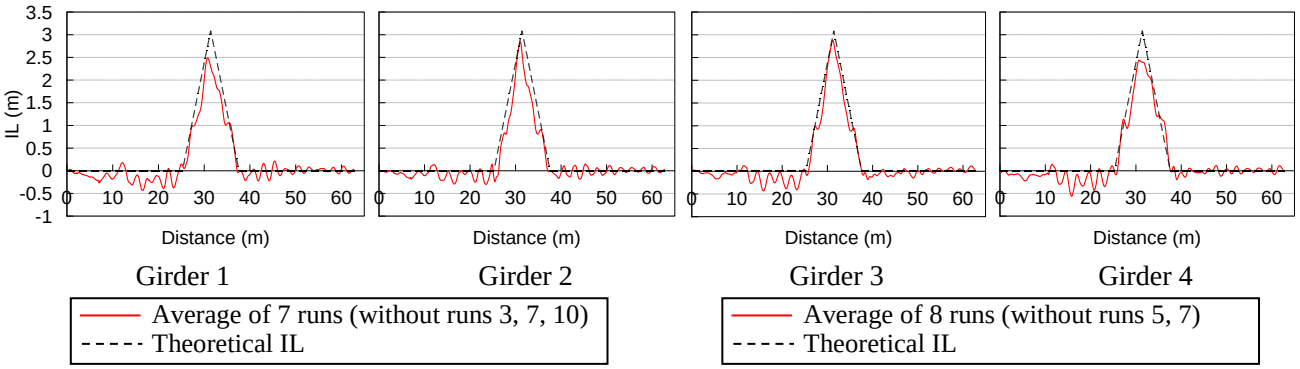

Fig. 12 ILs of all four girders

Calculation of Axle Weights

BWIM analysis presents an inverse-type problem in that the structural response (strain) is measured, but the live loads causing this response need to be determined. In order to determine the axle weights, a least-square method was applied to minimize the error between the measured response of the passing vehicle and the predicted response. In this manner, a simultaneous set of equations could be established, and the axle weights of passing vehicles could be obtained.

With the calculated ILs of each girder as references, the axle weights could be calculated in terms of the measured bridge response. For this procedure, the bridge was considered as a whole to undertake the vehicle loads, taking into account the transverse distribution of the wheel loads. At time step k, the bending moment of girder j, M_k^j, was given as (Fig. 7):

$$M_k^j = E_j Z_j \varepsilon_{j,k}^t \tag{24}$$

The total bending moment across the bridge section, M_k, at time step k was expressed by

$$M_k = \sum_{j=1}^{g} M_k^j = \sum_{j=1}^{g} E_j Z_j \varepsilon_{j,k}^t = \sum_{j=1}^{g} B_j \varepsilon_{j,k}^t \tag{25}$$

where $B_j = E_j Z_j$; $\varepsilon_{j,k}^t$ was the predicted strains at the jth girder at time step k.

When a calibration truck with N known axle weights, P_1, P_2, $\cdots, P_N$, passed over the bridge, according to the measured bridge response (from Table 3), $Q_1, Q_2, \cdots, Q_g$ was obtained. Thus, the ith axle load on the jth girder was $P_i \times Q_j$ ($i = 1, 2, \cdots, N$; $j = 1, 2, \cdots, g$) (Fig. 7). For the K scans of data acquisition, the IL coordinates of jth girder at time step k were $I_{j,k}$ ($j = 1, \cdots, g; k = 1, \cdots, K$). Considering all the girders together, at time step k, the corresponding theoretical load effect (bending moment, M_k) was

$$M_k = \sum_{j=1}^{g} \sum_{i=1}^{N} (P_i \times Q_j \times I_{j,(k-C_i)}) \tag{26}$$

Integration of Eq. (25) and Eq. (26) led to

$$\{B\}^T \{\varepsilon^t\}_k = \{Q\}^T [IL_k] \{P\} \tag{27}$$

where

$$\{B\} = \begin{Bmatrix} B_1 \\ B_2 \\ \vdots \\ B_g \end{Bmatrix}; \quad \{\varepsilon^t\}_k = \begin{Bmatrix} \varepsilon_{1k}^t \\ \varepsilon_{2k}^t \\ \vdots \\ \varepsilon_{gk}^t \end{Bmatrix}; \quad \{Q\} = \begin{Bmatrix} Q_1 \\ Q_2 \\ \vdots \\ Q_g \end{Bmatrix}; \quad \{P\} = \begin{Bmatrix} P_1 \\ P_2 \\ \vdots \\ P_N \end{Bmatrix} \tag{28a}$$

$$[IL_k]=\begin{bmatrix} I_{1,k} & I_{1,(k-C_2)} & \cdots & I_{1,(k-C_N)} \\ I_{2,k} & I_{2,(k-C_2)} & \cdots & I_{2,(k-C_N)} \\ \vdots & & & \\ I_{g,k} & I_{g,(k-C_2)} & \cdots & I_{g,(k-C_N)} \end{bmatrix}=[\{I\}_k \quad \{I\}_{k-C_2} \quad \cdots \quad \{I\}_{k-C_N}] \tag{28b}$$

The total IL coordinates for all girders at all *K* time steps could be written as:

$$[I]=\begin{bmatrix} [IL_1] \\ [IL_2] \\ \vdots \\ [IL_K] \end{bmatrix}=\begin{bmatrix} \{I\}_1 & \{I\}_{1-C_2} & \cdots & \{I\}_{1-C_N} \\ \{I\}_2 & \{I\}_{2-C_2} & \cdots & \{I\}_{2-C_N} \\ \vdots & & & \\ \{I\}_K & \{I\}_{K-C_2} & \cdots & \{I\}_{K-C_N} \end{bmatrix} \tag{29}$$

According to Eq. (27), the theoretical bridge response at time step *k* was defined as:

$$L_k^t=\{B\}^T\{\varepsilon^t\}_k=P_1\{I\}_k^T\{Q\}+P_2\{I\}_{k-C_2}^T\{Q\}+\cdots+P_N\{I\}_{k-C_N}^T\{Q\}=\sum_{i=1}^{N}P_i\{I\}_{k-C_i}^T\{Q\} \tag{30}$$

Thus, for all time steps, one had

$$\{L^t\}=P_1[I^{C_1}]\{Q\}+P_2[I^{C_2}]\{Q\}+\cdots+P_N[I^{C_N}]\{Q\}=\sum_{i=1}^{N}P_i\left\{I^{C_i}\right\}_{k-C_i}^T\{Q\} \tag{31}$$

where

$$\{L^t\}=[L_1^t \quad L_2^t \quad \cdots \quad L_K^t]^T \tag{32}$$

and

$$\left[I^{C_i}\right]=\begin{bmatrix} \{I\}_{1-C_i}^T \\ \{I\}_{2-C_i}^T \\ \vdots \\ \{I\}_{K-C_i}^T \end{bmatrix}=\begin{bmatrix} I_{1,1-C_i} & I_{2,1-C_i} & \cdots & I_{g,1-C_i} \\ I_{1,2-Ci} & I_{2,2-C_i} & \cdots & I_{g,2-C_i} \\ \vdots & \vdots & \vdots & \vdots \\ I_{1,K-C_i} & I_{2,K-C_i} & \cdots & I_{g,K-C_i} \end{bmatrix} \quad (i=1,\cdots,N) \tag{33}$$

Similarly, the measured bridge response was given by:

$$L_k^m=\{B\}^T\{\varepsilon^m\}_k \tag{34}$$

An error function was thus defined as:

$$E=\sum_{k=1}^{K}(L_k^t-L_k^m)^2 \tag{35}$$

In matrix form, the error function could be written as:

$$E=\left\{\{L^m\}-\{L^t\}\right\}^T\left\{\{L^m\}-\{L^t\}\right\} \tag{36}$$

where $\{L^m\}=[L_1^m \quad L_2^m \quad \cdots \quad L_K^m]^T$ was a vector of the measured bridge response, with each element illustrated as $L_k^m=B_1\varepsilon_{1,k}^m+B_2\varepsilon_{2,k}^m+\cdots+B_g\varepsilon_{g,k}^m$ ($k=1,\cdots,K$); and $\{L^t\}=[L_1^t \quad L_2^t \quad \cdots \quad L_K^t]^T$ was a vector of predicted bridge response.

Substituting Eq. (31) into Eq. (36) and differentiating the resulting error function *E* with respect to the *l*th axle weight, P_l, yielded

$$\frac{\partial E}{\partial P_l}=2\{Q\}^T\left[I^{C_1}\right]^T\left(\sum_{i=1}^{N}P_i\left[I^{C_i}\right]\{Q\}-\{L^m\}\right) \quad (i=1,\cdots,N,\ \ j=1,\cdots,N) \tag{37}$$

Minimizing the error function with respect to the vector of axle weights resulted in:

$$\frac{\partial E}{\partial P_l}=0 \qquad (l=1,\cdots,N) \tag{38}$$

and furthermore:

$$\{Q\}^T \left[I^{C_l}\right]^T \sum_{i=1}^{N} P_i \left[I^{C_i}\right]\{Q\} = \{Q\}^T \left[I^{C_l}\right]^T \{L^m\} \qquad (l = 1, \cdots, N). \tag{39}$$

By assuming

$$F_{ij} = \{Q\}^T \left[I^{C_i}\right]^T \left[I^{C_j}\right]\{Q\}, \quad M_i = \{Q\}^T \left[I^{C_i}\right]^T \{L^m\}, \quad i = 1, \cdots, N;\ j = 1, \cdots, N \tag{40}$$

Then

$$[F]\{P\} = \{M\} \tag{41}$$

where

$$[F] = \begin{bmatrix} F_{11} & F_{12} & \cdots & F_{1N} \\ F_{21} & F_{22} & \cdots & F_{2N} \\ \vdots & \vdots & \vdots & \vdots \\ F_{N1} & F_{N2} & \cdots & F_{NN} \end{bmatrix}; \{P\} = \begin{Bmatrix} P_1 \\ P_2 \\ \vdots \\ P_N \end{Bmatrix}; \{M\} = \begin{Bmatrix} M_1 \\ M_2 \\ \vdots \\ M_N \end{Bmatrix} \tag{42}$$

$$\{P\} = [F]^{-1}\{M\} \tag{43}$$

From equation (43), the axle loads could be obtained, and the GVW could be derived by

$$GVW = \sum_{i=1}^{N} P_i \tag{44}$$

Field Demonstration of the Algorithm in Predicting Axle Weights

To evaluate the proposed algorithm in identifying the axle weights of moving vehicles, the averaged ILs were used to calculate the corresponding axle weights (Fig. 12), taking the repeated ten runs in Lane 1 as a reference. Zhao (2010) demonstrated that, in order to improve the accuracy of axle weight calculations, the scan numbers of measured strain data should cover the entire process of a vehicle passing over an instrumented bridge. Herein, we selected the case that adding 100 samplings (about $100/512 = 0.2s$) before the vehicle approached the bridge and after the vehicle left the bridge to cover the process of the abrupt changes for the vehicle approaching or leaving the bridge. Table 5 illustrates the percentage errors of calculated axle weights of each run on Lane 1 in comparison with the static measurements. As seen from the original collected dynamic response for all the four girders (not included for the sake of brevity, see Zhao (2010)), Run 7 on Lane 1 was obviously different from other runs and the strain data of girder 1 appeared erratic including jumps and significant deviation compared to other runs. For this reason, the identified axle weights from Run 7 (Lane 1) was not satisfactory, warranting further investigation into the cause of deviation that was beyond the scope of the paper.

Table 5 Axle weight comparison of different runs with vehicles on Lane 1 (%)

Item / Run	Proposed algorithm for BWIM system									BPWIM
	A1	A2	A3	A4	A5	SA	GOA1	GOA2	GVW	GVW
	(%)	(%)	(%)	(%)	(%)	A1	A2+A3	A4+A5	(%)	(%)
1	-6.9	2.5	-6.6	-7.2	-0.7	-6.9	-2.1	-4.0	-3.6	2.3
2	0.3	-1.3	-0.5	1.4	-7.7	0.3	-0.8	-3.1	-1.7	3.5
3	-3.3	5.6	-7.7	-1.4	-4.9	-3.3	-1.2	-3.1	-2.3	2.9
4	11.2	-12.3	15.9	6.9	-3.4	11.2	2.0	1.8	3.2	10.0
5	12.0	-3.2	7.2	3.7	1.9	12.0	2.1	2.8	3.8	-2.7
6	21.6	11.8	-6.7	11.5	0.8	21.6	2.6	6.2	6.7	4.1
7	*30.5*	*1.3*	*6.1*	*24.0*	*-13.9*	*30.5*	*3.7*	*5.2*	*7.8*	-7.4
8	18.9	4.6	-1.2	13.6	-3.6	18.9	1.7	5.0	5.5	-10.0
9	19.7	-1.9	3.0	19.4	-8.8	19.7	0.5	5.4	5.3	-4.9
10	19.5	1.4	2.1	16.0	-8.0	19.5	1.7	4.0	5.1	-7.0
Mean	10.33	0.80	0.61	7.10	-3.82	10.33	1.19		2.44	-0.20
St. dev.	10.95	6.72	7.62	8.75	3.91	10.95	3.04		3.89	6.35

Note: (1) Run 7 was not included in the calculation of the mean and standard deviation.

Table 6 lists the percentage errors of calculated axle weights of each run on Lane 2 in comparison with the static measurements. Again, from the original collected dynamic response for all the four girders, it was found that the collected data for all the four girders of Run 7 (Lane 2) was totally different from other runs. Since the collected data of Run 7 (Lane 2) was inaccurate and not reliable, this run should be removed from the calculation. The results for Run 7 (Lane 2) was listed in Table 6 just for comparison. As can be seen from Table 3, the load distribution of this run was also listed for reference.

Table 6. Axle weight comparison of different runs with vehicles on Lane 2 (%)

Item	Proposed algorithm for BWIM system									BPWIM
Run	A1	A2	A3	A4	A5	SA	GOA1	GOA2	GVW	GVW
	(%)	(%)	(%)	(%)	(%)	A1	A2+A3	A4+A5	(%)	(%)
1	14.2	3.2	4.1	-4.0	8.3	14.2	3.7	2.1	4.3	5.4
2	16.3	4.0	5.2	4.6	2.4	16.3	4.6	3.5	5.6	-2.8
3	20.7	-9.3	17.2	2.1	4.2	20.7	3.9	3.1	5.7	8.4
4	15.9	0.9	8.1	1.7	8.3	15.9	4.5	5.0	6.2	10.9
5	10.6	-22.4	37.2	1.7	6.9	10.6	7.8	4.3	6.6	11.3
6	7.8	-6.9	28.3	5.7	9.3	7.8	10.9	7.5	8.9	-8.1
7	*19.7*	*-46.9*	*-22.1*	*-64.6*	*-65.0*	*19.7*	*-34.3*	*-64.8*	*-40.7*	-9.1
8	-0.4	-4.3	13.7	-0.2	1.6	-0.4	4.8	0.7	2.2	-15.7
9	19.1	-14.9	27.3	-11.6	16.4	19.1	6.1	2.3	6.0	6.5
10	8.2	-10.5	15.7	7.4	-2.3	8.2	2.8	2.6	3.4	-12.5
Mean	12.49	-6.69	17.42	0.82	6.12	12.49	4.46		5.43	0.38
St. dev.	6.62	8.74	11.39	5.73	5.42	6.62	2.42		1.94	10.39

Note: (1) Run 7 was not included in the calculation of the mean and standard deviation.

To assess the relative accuracies of the BWIM and BPWIM systems, the results calculated by the proposed algorithm for the BWIM system were compared to results acquired from the BPWIM system, which was also listed in Table 5 and Table 6, respectively. For simplicity, only GVW results for the BPWIM system are presented. In Tables 5 and 6, 'A1-A5' represents the axle number of the calibration vehicle from the front to the rear; 'SA' represents a single axle; 'GOA' refers to the group of axles; and, for the means and standard deviations of A1, A2, A3, A4, A5, SA and GVW, the number was 9 (without run 7); that for GOA was 18 (without run 7).

As seen in Table 5, for the ten runs on Lane 1, except for run 7, the calculated axle weights based on the proposed algorithm were acceptable. The percentage errors of SA were less than 20%, that for GOA was less than 6.2%, and that for GVW was less than 6.7%.

As can be seen from Table 6, for the ten runs on Lane 2, the results of Run 7 was significantly less than the static measurements, since the collected data of Run 7 was inaccurate and not reliable, and the signals of this run was considerably smaller than other runs. For the other nine runs, the percentage errors of SA were less than 20%, that for GOA was less than 10.9%, and that for GVW was less than 8.9%.

When vehicles was on Lane 1, Girders 1 and 2 undertake almost 80% load, Girder 3 bears a portion of load around 20%, and Girder 4 bears load less than 5% (Table 3). Considering this fact this paper conducts comparison analysis including the following three different cases: Case 1 - considering all the four girders; Case 2 - considering only girders 1, 2, and 3; Case 3 - considering only girders 1 and 2. The details of each case are as following.

When considering all the four girders of the instrumented bridge, Eq. (28a) and Eq. (28b) could be written as

$$\{B\}=\begin{Bmatrix}B_1\\B_2\\B_3\\B_4\end{Bmatrix};\{\varepsilon^t\}_k=\begin{Bmatrix}\varepsilon^t_{1k}\\\varepsilon^t_{2k}\\\varepsilon^t_{3k}\\\varepsilon^t_{4k}\end{Bmatrix};\{Q\}=\begin{Bmatrix}Q_1\\Q_2\\Q_3\\Q_4\end{Bmatrix};[IL_k]=\begin{bmatrix}I_{1,k} & I_{1,(k-C_2)} & \cdots & I_{1,(k-C_N)}\\I_{2,k} & I_{2,(k-C_2)} & \cdots & I_{2,(k-C_N)}\\I_{3,k} & I_{3,(k-C_2)} & \cdots & I_{3,(k-C_N)}\\I_{4,k} & I_{4,(k-C_2)} & \cdots & I_{4,(k-C_N)}\end{bmatrix};\{P\}=\begin{Bmatrix}P_1\\P_2\\\vdots\\P_N\end{Bmatrix} \tag{45}$$

For a vehicle in Lane 1, the transverse distribution of girder 4 was small (less than 5%) (Table 3). Without considering the transverse distribution of wheel load on girder 4, and using the corresponding percentages of girders 1, 2, and 3 to represent all the load effects, then Eq. (27) could be changed to:

$$\{B\}^T\{\varepsilon^t\}_k=\left(\{Q\}^T[IL_k]\{P\}\right)/(1-Q_4) \tag{46}$$

where $\{B\}$, $\{\varepsilon^t\}_k$, and $\{P\}$ were same as those in Eq. (45), but

$$\{Q\}=\begin{Bmatrix}Q_1\\Q_2\\Q_3\end{Bmatrix};[IL_k]=\begin{bmatrix}I_{1,k} & I_{1,(k-C_2)} & \cdots & I_{1,(k-C_N)}\\ I_{2,k} & I_{2,(k-C_2)} & \cdots & I_{2,(k-C_N)}\\ I_{3,k} & I_{3,(k-C_2)} & \cdots & I_{3,(k-C_N)}\end{bmatrix} \quad (47)$$

Since the process was the same as the calculation considering the distribution factor of all the four girders, the axle load could be calculated as

$$\{P\}=\left([F]^{-1}\{M\}\right)\times(1-Q_4) \quad (48)$$

The elements of matrix $[F]$ and vector $\{M\}$ were different from those in Eq. (41), because only the distribution and corresponding ILs of girders 1, 2, and 3 were considered.

For a vehicle in Lane 1, the vehicle weight was undertaken mainly by girders 1 and 2. For comparison only, without considering the contribution of girders 3 and 4, and using the corresponding percentages for girders 1 and 2 to represent all the load effects, Eq. (27) could be rewritten as:

$$\{B\}^T\{\varepsilon^t\}_k=\left(\{Q\}^T[IL_k]\{P\}\right)/(1-Q_3-Q_4) \quad (49)$$

where $\{B\}$, $\{\varepsilon^t\}_k$, and $\{P\}$ were same as those in Eq. (45), but

$$\{Q\}=\begin{Bmatrix}Q_1\\Q_2\end{Bmatrix};[IL_k]=\begin{bmatrix}I_{1,k} & I_{1,(k-C_2)} & \cdots & I_{1,(k-C_N)}\\ I_{2,k} & I_{2,(k-C_2)} & \cdots & I_{2,(k-C_N)}\end{bmatrix} \quad (50)$$

Similarly, the axle weights could be calculated as

$$\{P\}=\left([F]^{-1}\{M\}\right)\times(1-Q_3-Q_4) \quad (51)$$

The elements of matrix $[F]$ and vector $\{M\}$ were different from those in Eq. (41), because the distribution and corresponding ILs of only girders 1 and 2 were considered.

For the case that does not take into account girder 4 (considering only girders 1, 2, and 3) and the case that does not consider girders 3 and 4, the calculated axle weights are calculated (Table 7). Table 8 shows a comparison of the three different cases. For brevity, Table 7 and Table 8 just lists the results of Lane 1.

Table 7. Axle weight comparison considering two different cases with vehicles on Lane 1

Item	Proposed algorithm for the BWIM system																		BPWIM
	A1		A2		A3		A4		A5		SA (%)		GOA (%)				GVW		GVW
Run	(%)		(%)		(%)		(%)		(%)		A1		A2+A3		A4+A5		(%)		(%)
	①	②	①	②	①	②	①	②	①	②	①	②	①	②	①	②	①	②	
1	-6.5	-4.9	1.6	5.0	-5.6	-5.2	-7.4	-5.3	-0.1	0.9	-6.5	-4.9	-2.0	-0.2	-3.8	-2.2	-3.5	-1.8	2.3
2	0.7	2.7	-2.6	0.1	0.6	1.6	0.9	2.9	-7.1	-6.0	0.7	2.7	-1.0	0.9	-3.1	-1.5	-1.7	0.0	3.5
3	-2.8	-0.9	4.2	7.2	-6.6	-6.0	-1.9	0.3	-4.2	-3.2	-2.8	-0.9	-1.3	0.5	-3.1	-1.5	-2.3	-0.6	2.9
4	11.5	13.5	-11.9	-8.5	17.0	17.5	7.0	9.1	-2.6	-1.3	11.5	13.5	2.8	4.7	2.3	3.9	3.8	5.6	10.0
5	12.3	14.0	-4.0	0.1	8.2	8.2	3.5	6.1	2.5	3.2	12.3	14.0	2.2	4.2	3.0	4.7	4.0	5.8	-2.7
6	21.9	24.0	11.4	14.3	-5.7	-4.7	11.5	13.5	1.2	2.7	21.9	24.0	2.9	4.9	6.4	8.1	7.0	8.9	4.1
7	*31.0*	*33.8*	*-0.4*	*2.1*	*7.5*	*8.8*	*23.3*	*24.9*	*-13.0*	*-11.2*	*31.0*	*33.8*	*3.5*	*5.4*	*5.3*	*7.0*	*7.9*	*9.8*	-7.4
8	19.2	21.8	4.2	6.6	-0.1	1.2	13.4	14.7	-3.0	-0.7	19.2	21.8	2.0	3.9	5.3	7.0	5.7	7.6	-10.0
9	19.9	22.4	-3.0	-1.2	4.0	5.8	19.0	21.9	-8.4	-7.8	19.9	22.4	0.4	2.3	5.4	7.2	5.3	7.1	-4.9
10	20.0	22.6	1.1	3.4	3.2	4.7	15.9	17.3	-7.3	-5.3	20.0	22.6	2.2	4.0	4.4	6.1	5.5	7.4	-7.0
Mean	10.69	12.80	0.11	3.00	1.67	2.57	6.88	8.94	-3.22	-1.94	10.69	12.80	1.39 (①)		3.17 (②)		2.64	4.44	-0.92
St. dev.	10.90	11.18	6.54	6.41	7.63	7.58	8.81	8.76	3.90	3.90	10.90	11.18	3.14 (①)		3.17 (②)		4.00	4.08	6.41

Note: (1) Column ① contains values for the case considering only girders 1, 2, and 3; (2) Column ② contains values for the case considering only girders 1 and 2; and (3) Run 7 was not included in the calculation of mean and standard deviation.

The results in Tables 6, 7 and 8 demonstrate that the accuracy for GVW was acceptable for enforcement screening based on the proposed algorithm in IL calculation and axle weight identification.

Table 8. Summary of comparisons of axle weights for the three cases with vehicles on Lane 1

Item	Number	Considering all 4 girders		Considering only girders 1, 2 and 3		Considering only girders 1 and 2	
		Mean	St. dev.	Mean	St. dev.	Mean	St. dev.
		(%)	(%)	(%)	(%)	(%)	(%)
GVW	9	2.44	3.89	2.64	4.00	4.44	4.08
GOA	18	1.19	3.04	1.39	3.14	3.17	3.17
SA	9	10.33	10.95	10.69	10.90	12.80	11.18

Note: Run 7 was not considered.

Considering girders 1, 2 and 3, or only girders 1 and 2, the proposed algorithm also exhibits acceptable accuracy in identifying axle weights, especially for GOA and GVW (Table 7). The results for the case considering all the four girders demonstrated essentially the same accuracy as those for the case considering girders 1, 2, and 3 (Table 7). Both cases showed a slightly better accuracy than the case considering only girders 1 and 2 (Tables 7 and 8). One reason was that, as the vehicle crossed the bridge in Lane 1, the distributed wheel load on girder 4 was extremely small. Another reason was that, since the proposed algorithm in axle weight identification took the bridge response (strain) considering all the girders as an error function variable, calculations considering transverse distribution of wheel loads on all the four girders would show better results than those considering only the girders under passing vehicles.

Based on experience with the bridges considered, the authors would propose the following rule of thumb. If the bridge has n number of girders, and if the contribution of the girders is less than $1/(2n)$ of the total response (half of the average percentage of the total response), the response of those very girders should be removed from the calculation. For example, for a bridge with ten girders, if the percentage of the response of the girders is less than 5% (half of the average percentage of each girder), those girder responses should be removed from the calculation.

As seen from Table 5, comparisons with static weights on a one-to-one basis for both BWIM predictions and BPWIM measurements show that the GVW percentage error of vehicles on Lane 1 for BWIM is less than 6.7%, and that for BPWIM is below 10%. The percentage error of vehicles on Lane 2 for BWIM have generally fallen below a 10%, while that for BPWIM is almost within 15.7%. The predicted GVW by BWIM of vehicles on Lane 1 has a mean of 2.44% and a standard deviation of 3.89%, and that by BPWIM has a mean of -0.92% and a standard deviation of 6.41%. For vehicles on Lane 2, the predicted GVW by BWIM has a mean of 5.43% and a standard deviation of 1.94%, and that by BPWIM has a mean of 0.38% and a standard deviation of 10.39%. With a standard deviation of 3.89% (Lane 1) and 1.94% (Lane 2) , BWIM results demonstrated substantial repeatability in identifying GVW of moving vehicles. Field tests demonstrated that the BWIM systems showed similar levels of accuracy to their conventional BPWIM counterparts. However, BWIM systems exhibit advantages over conventional BPWIM systems due to their portability, cost-effectiveness, and useful information on existing bridges including bridge capacity and hence safety.

Conclusions

This paper introduces an innovative BWIM system using an instrumented bridge as a large scale to continuously collect vehicle information of passing vehicles, including speed, axle spacing, and axle weights. The mathematical equations to calculate the ILs and axle weights considering realistic transverse wheel load distribution are presented. The proposed algorithm was implemented by a computer program in MATLAB. Field testing of a concrete slab-girder bridge on highway US-78 in Alabama was carried out to test and evaluate the accuracy of the proposed algorithm in the identification of axle weights, in comparison with static weights and with weight measurements from a BPWIM system for moving heavy vehicles. The key findings are as follows:

(1) In obtaining transverse distribution of wheel loads based on the measured bridge responses, the proposed algorithm is effective and accurate, and can be applied as a reference for IL calculation and axle weight identification.

(2) In the calculation of ILs, the algorithm accounts for realistic bridge behavior by considering the transverse distribution of wheel loads and acquires the ILs of each girder. Based on a comparison of the measured responses of each girder and the predicted theoretical responses from the calculated ILs, the algorithm is effective in the calculation of ILs. The calculated ILs of each girder, considering the transverse distribution of wheel loads, represents the 2-dimensional behavior of the bridge.

(3) Field testing of the bridge on highway US-78 demonstrates that the modified Moses algorithm for axle weight identification, which includes the transverse distribution of wheel loads and includes the 2-dimensional behavior of the bridge, is suitable for simple supported concrete slab-girder bridges, which are typical in Alabama and other states in the U.S. Considering all the girders together, the mean percentage error of the predicted SA, GOA and GVW of vehicles on Lane 1 are 10.33%, 1.19% and 2.44%, respectively, relative to static measurements; those of vehicles on Lane 2 are 12.49%, 4.46%, and 5.43%, respectively. The standard deviation of predicted SA, GOA and GVW of vehicles on Lane 1 are 10.95%, 3.04%, and 3.89%, respectively; those of vehicles on Lane 2 are 6.62%, 2.42%, and 1.94%, respectively, illustrating that the proposed algorithm in axle weight identification is repeatable, effective, and accurate.

(4) Based on the comparisons with static weights on a one-to-one basis for both BWIM and BPWIM systems, BWIM system results obtained with the proposed algorithm demonstrate that BWIM systems show similar levels of accuracy as their conventional BPWIM counterparts. However, the BWIM system provides advantages over conventional BPWIM due to its accuracy, portability, cost-effectiveness, and useful information on existing bridges including bridge capacity and hence safety.

Acknowledgements

This research was supported by National Natural Science Foundation of China (51178178), National Science Foundation (1100742), Science Foundation Ireland, Hunan Provincial Natural Science Foundation of China (13JJ2019), Scientific Research Foundation for the Returned Overseas Chinese Scholars, the State Education Ministry (521294021), Research Fund for the Doctoral Program of Higher Education of China (20110161120025). These programs are gratefully acknowledged.

References

AASHTO. (2012). *AASHTO LRFD Bridge Design Specification*. 6th Ed., American Association of State Highway and Transportation Officials, Washington D.C.

COST 323. (1999). *European Specification on Weigh-in-Motion of Road Vehicles*, Final Report, Appendix I, Ver. 3.0, EUCO-COST/323/8/99, LCPC, Paris, August. URL: http://wim.zag.si/reports/specifications/ WIM specs.pdf

Dempsey, A.T., O'Brien, E.J. and O'Connor, J.M. (1995), A bridge weigh-in-motion system for the determination of gross vehicle weights, *Post proceedings of first European conference on weigh-in-motion of road vehicles* (eds.) B. Jacob et al., ETH, Zurich, pp. 239-249

González, A. (2010), *Development of a Bridge Weigh-In-Motion System: A technology to convert the bridge response to the passage of traffic into data on vehicle configurations, speeds, times of travel and weights*, May, Lambert Academic Publishing

González, A. and O'Brien, E.J. (1998), The development of a dynamic bridge weigh-in-motion algorithm, *Pre-proceedings of 2nd European Conference on Weigh-in-Motion of Road Vehicles*, Editors, E.J. O'Brien and B. Jacob, Lisbon, European Commission, Luxembourg, pp. 445-452

González, A. and O'Brien, E.J. (2002), Influence of dynamics on accuracy of a bridge weigh-in-motion system. *Proceedings of 3rd International Conference on Weigh-In-Motion (ICWIM3)*, Orlando, Editors, Jacob B., McCall B. and O'Brien, E.J. pp. 189-198

González, A., Dowling, J., O'Brien, E.J. and Žnidarič, A. (2012), Testing of a bridge weigh-in-motion algorithm utilising multiple longitudinal sensor locations, Journal of Testing and Evaluation (JTE), 40(6): 961-974

Jacob, B., Hannachi, H. and Ieng, S.S. (2010), Bridge weigh-in-motion on steel orthotropic decks – Millau viaduct and Autreville bridge, *Proceedings of the Fifth International IABMAS Conference*, Edited by Frangopol,

D.M., Sause, R. and Kusko, C.S., CRC Press 2010, Philadelphia, USA, p 209

Leming, S.K. and Stalford, H.L. (2003), Bridge weigh-in-motion system development using superposition of dynamic truck/ static bridge interaction, *Proceedings of the American Control Conference*, Denver, Colorado, June 4-6, pp. 815-820

Matui, S. and El-Hakim, A. (1989), Estimation of axle loads of vehicle by crack opening of RC slab, *Journal of Structural Engineering, JSCE*, pp.407-418 (in Japanese)

McNulty, P. and O'Brien, E.J. (2003). Testing of bridge weigh-in-motion system in a sub-Arctic climate. *Journal of Testing and Evaluation* 31(6): 497-506

Moses, F. (1979), Weigh-in-motion system using instrumented bridges. *Transportation Engineering Journal (ASCE)*, 105: 233-249

O'Brien E.J., Quilligan, M.J. and Karoumi, R. (2006). Calculating an IL form direct measurements. *Proceedings of the Institution of Civil engineers, Bridge engineering* 159(1):31-34

O'Brien, E.J., Žnidarič, A. and Dempsey, A.T. (1999), Comparison of two independently developed bridge weigh-in-motion systems, *Heavy Vehicle Systems, International Journal of Vehicle Design*, 6(1-4): 147-162

Ojio, T., Yamada, K. and Shinkai, H. (2000), BWIM systems using truss bridges, *Bridge management four*, Editors, Ryall, M.J., Parker, G.A.R. and Harding, J.E., Thomas Telford, University of Surrey, UK, pp. 378-386

Peters, R.J. (1984), AXWAY- a system to obtain vehicle axle weights, *Proceedings 12th ARRB conference*, Hobart, Australia, 12(1): 17-29.

Peters, R.J. (1986), An unmanned and undetectable highway speed vehicle weighing system, *Proceedings 13th ARRB conference*, Adelaide, Australia, 13(6): 70-83

Quilligan, M., Karoumi, R. and O'Brien, E.J. (2002), Development and testing of a 2-dimensional multi-vehicle bridge-WIM algorithm, *3rd International Conference on Weigh-in-Motion (ICWIM3)*, Editors, Jacob, B., McCall, B. and O'Brien, E.J., Orlando, pp. 199-208

Rowley, C.W., González, A., O'Brien, E.J. and Žnidarič, A. (2008). Comparison of conventional and regularized bridge weigh-in-motion algorithms. *5th International Conference on Weigh-in-Motion (ICWIM5)*, Editors, Jacob, B., O'Brien, E.J., O'Connor, and Bouteldja, M., LCPC Publications, Paris, pp. 221-230

Snyder, R.E. (1992), *Field trials of low-cost bridge WIM, in publication* FHWA-SA-92-014, Washington DC.

Xiao, Z.G., Yamada, K., Inoue, J. and Yamaguchi, K. (2006), Measurement of truck axle weight by instrumenting longitudinal ribs of orthotropic bridge, *Journal of Bridge Engineering (ASCE)*, 11(5): 526-532

ZAG, Cestel (2005), *SiWIM Bridge Weigh-in-Motion Manual*, 3rd Edition, May, Slovenia

Zhao, H. (2010), *Bridge weigh-in-motion for bridge safety and maintenance. Ph.D. Dissertation*, Department of Civil, Construction, and Environmental Engineering, University of Alabama at Birmingham, Alabama, USA

Žnidarič, A. and Baumgartner, W. (1998), Bridge weigh-in-motion systems – an overview, *Pre-proceedings of the 2nd European conference on weigh-in-motion*, Editors: O'Brien, E.J. and Jacob, B., Lisbon, Portugal, pp.139-152

Žnidarič, A., Lavrič, I and Kalin, J. (2002), The next generation of bridge weigh-in-motion systems, *Proceedings of Third International Conference on Weigh-In-Motion (ICWIM3)*, Editors, Jacob, B. and O'Brien, E.J., Orlando, USA, pp. 219-229

Žnidarič, A., Lavrič, I and Kalin, J., and Kulauzovic, B. (2011), *SiWIM Bridge Weigh-in-Motion Manual*, 4th Edition, ZAG Ljubljana.